Pharmaceutical Sciences and Drug Design
ISSN: 3062-4428
2021, Volume 1, Page No: 179-193

Available online at: www.galaxypub.co/page/journals

Galaxy Publication

Discovery of Two Flavonoid Compounds as Novel and Safe Inhibitors of Kynurenine Aminotransferase II through Computational and Experimental Analysis

Camille Bernard[1], Julien Martin[2], Lucas Moreau[1]*, Sophie Laurent[2]

[1]Department of Medicinal Chemistry, Faculty of Pharmacy, University of Strasbourg, Strasbourg, France.
[2]Department of Pharmaceutical Sciences, Faculty of Pharmacy, University of Lyon, Lyon, France.

***E-mail** ✉ lucas.moreau@gmail.com

Received: 07 September 2021; **Revised:** 02 December 2021; **Accepted:** 07 December 2021

ABSTRACT

Kynurenine aminotransferase II (KAT-II) serves as a promising therapeutic target for managing various disorders associated with elevated levels of kynurenic acid (KYNA). Existing KAT-II inactivators, while effective, frequently cause unwanted side effects stemming from their irreversible mode of action. The objective of this investigation was to discover effective and safer KAT-II inhibitors through integrated computational modeling and experimental validation in vitro. Top candidate compounds were selected via virtual screening, MM/GBSA free energy calculations, and molecular dynamics simulations. These were subsequently assessed using enzyme kinetic assays and cytotoxicity testing in cell culture. Among the screened compounds, herbacetin and (-)-Epicatechin demonstrated superior performance. Their Glide docking scores were −8.66 kcal/mol and −8.16 kcal/mol, respectively, with MM/GBSA binding free energies of −50.30 kcal/mol and −51.35 kcal/mol. These values outperformed the reference inhibitor PF-04859989, which recorded a docking score of −7.12 kcal/mol and a binding energy of −38.41 kcal/mol. ADMET predictions indicated that the lead compounds possess desirable pharmacokinetic properties, acceptable bioavailability, and low toxicity risk, suggesting their suitability for further development. Kinetic analyses confirmed that both herbacetin and (-)-Epicatechin act as reversible inhibitors with a competitive mechanism. Their IC50 values were determined to be 5.98 ± 0.18 µM and 8.76 ± 0.76 µM, respectively. Additionally, MTT assays showed no impact on HepG2 cell viability at concentrations required for effective KAT-II inhibition. The findings indicate that herbacetin and (-)-Epicatechin are effective inhibitors of KAT-II and represent viable leads for advancing novel inhibitor design.

Keywords: Herbacetin, (-)-Epicatechin, KAT-II inhibition, Molecular docking

How to Cite This Article: Bernard C, Martin J, Moreau L, Laurent S. Discovery of Two Flavonoid Compounds as Novel and Safe Inhibitors of Kynurenine Aminotransferase II through Computational and Experimental Analysis. Pharm Sci Drug Des. 2021;1:179-93. https://doi.org/10.51847/YNQJwSy2py

Introduction

Tryptophan (TRP), an essential amino acid, undergoes metabolism to yield various biologically active metabolites. Serotonin is perhaps the most recognized product, arising from a distinct biosynthetic route. Nevertheless, the majority—approximately 95%—of dietary TRP is converted to kynurenine (KYN) and subsequent derivatives, including KYNA, primarily through the action of KAT isoforms. Elevated brain concentrations of kynurenic acid (KYNA) have been implicated in schizophrenia and related central nervous system conditions [1, 2]. Consequently, agents modulating the kynurenine pathway (KP) hold promise for treating neurological disorders.

Within the human brain, KAT-II is primarily responsible for synthesizing KYNA, positioning it as a key target for pharmacological intervention [1, 3]. Prior efforts have yielded selective irreversible KAT-II inhibitors, including PF-04859989 and BFF-122. For instance, PF-04859989 has been shown to lower KYNA levels by up

to 50% in the rat prefrontal cortex and attenuate dopaminergic neuron activity in the midbrain [1, 4]. Although these agents show therapeutic potential for certain neurological conditions, their interaction with the cofactor pyridoxal-5-phosphate (PLP) raises concerns about off-target effects and safety [5, 6]. This highlights the demand for alternative inhibitors, ideally reversible and competitive, to mitigate such risks. Existing reversible options like S-ESBA and NS-1502 exhibit relatively weak potency (IC50 values of 1000 μM for S-ESBA and 315 μM for NS-1502) [6, 7]. More recently, BFF-816 has demonstrated KYNA reduction in vivo following kynurenine administration, though its selectivity across KAT isoforms remains incompletely characterized [6].

Numerous effective enzyme inhibitors originate from natural sources, particularly flavonoids, which are polyphenolic plant compounds renowned for their broad health-promoting effects. Flavonoids exhibit diverse bioactivities, including antimicrobial, antiviral, antioxidant, and anti-inflammatory properties, positioning them as valuable scaffolds for drug discovery [8, 9]. The present work adopts an innovative strategy by screening natural products to uncover novel KAT-II inhibitors—an underexplored direction in this domain [5, 10]. Through virtual screening of a focused natural compound library, followed by detailed ADME profiling and molecular dynamics assessment of binding stability, promising leads were identified. These were then validated experimentally for inhibitory efficacy and cellular safety, underscoring their potential to guide future therapeutic advancements.

Materials and Methods

Chemicals and reagents

Recombinant human KAT-II protein and associated buffers were purchased from R&D Systems, Bio-Techne (Abingdon Science Park, Abingdon, UK). The HepG2 cell line, solvents, and all other reagents—including herbacetin, (−)-epicatechin, and PF-04859989—were acquired from Sigma-Aldrich Chemie GmbH (Eschenstr., Taufkirchen, Germany).

Computational methods

Protein preparation and receptor grid generation

The crystal structure of human KAT-II (resolution: 2.89 Å; PDB ID: 4GDY) [11] was retrieved from the RCSB Protein Data Bank [12]. This structure comprises 439 amino acids and includes a bound co-crystal ligand (native inhibitor). Prior to docking, the Protein Preparation Wizard within the Maestro Schrödinger suite was employed to refine the structure. The PLP cofactor was excluded to avoid potential competition with candidate ligands at the active site [6]. Non-essential water molecules were deleted, hydrogen atoms were added, and partial charges were assigned using the OPLS-3e force field. The receptor grid was generated with an enclosing cubic box centered at coordinates (x = 4.15, y = 39.13, z = 26.61), and the maximum allowable ligand length for docking was set to 15 Å.

ligand preparation

A library of 480 natural compounds was assembled from the Sigma-Aldrich natural products collection (accessed on 23 April 2023; https://www.sigmaaldrich.com/DZ/en/products/chemistry-and-biochemicals/biochemicals/natural-products). Three-dimensional structures of these compounds, along with that of the reference inhibitor PF-04859989, were downloaded in SDF format from the PubChem database [13]. The library was subsequently filtered according to Lipinski and Veber rules [14, 15] using the Ligand Filtering module in Schrödinger, yielding 231 compliant compounds selected for virtual screening. Ligand preparation was performed with the LigPrep tool in Maestro Schrödinger, generating ionized states at physiological pH (7.0 ± 2.0) and relevant tautomeric forms for each molecule.

Virtual screening via molecular docking

In this research, a computational screening was performed using a collection of natural compounds sourced from the Sigma-Aldrich catalog to assess their ability to act as inhibitors of a key enzyme in the kynurenine pathway.

The selected phytochemicals were evaluated against KAT-II employing the Glide software from Schrödinger, LLC (New York, NY, USA, v2021.2). Docking of all plant-derived compounds was carried out in Glide XP (extra precision) mode [16]. The five highest-ranking compounds, considering only their optimal poses, were chosen according to docking scores and key molecular contacts with the target protein for subsequent evaluation.

Interaction analysis of the ligand-protein complexes was performed using the Pose Viewer tool in Maestro v12.8.117.

MMGBSA rescoring

Prime/MMGBSA computations were utilized to re-evaluate the docked ligands and estimate the relative binding free energies (ΔG bind) for each pose. These complexes then underwent energy minimization. The binding free energy (ΔG bind) for the five leading compounds was calculated based on the equation:

$$\Delta G \text{ (binding affinity)} = \Delta G \text{ (solvation energy)} + \Delta E \text{ (minimized energy)} + \Delta G \text{ (surface area energies)} \quad (1)$$

In this formula, ΔG (solvation energy) denotes the GBSA solvation energy difference between the inhibitor-KAT-II complex and the separate energies of the unbound KAT-II and the individual inhibitor. ΔE (minimized energy) refers to the energy difference between the complex and the combined energies of the protein with and without the ligand, while ΔG (surface area) accounts for the surface area energy difference between the complex and the summed values for the unbound protein and inhibitor.

Evaluation of drug-likeness and admet properties

The QikProp tool within the Schrödinger suite (Schrödinger, LLC, New York, NY, USA, v2021.2) was employed to assess the ADME characteristics and drug-like features of the chosen compounds, compared to the reference inhibitor, by examining compliance with Lipinski's rule of five (ROF) and various pharmacokinetic parameters, such as predicted octanol/water partition coefficient, human oral absorption, and Caco-2 cell permeability. Toxicity profiles were predicted using the ProTox-II online server [17].

Induced fit docking (IFD)

The induced fit docking approach was applied to account for flexibility in both the receptor and ligands, utilizing the IFD module in Maestro v12.8 (Schrödinger, LLC). This technique helps minimize inaccurate poses, yielding binding modes more aligned with actual biological interactions.

The two leading compounds were selected for IFD based on their XP docking scores, interaction patterns, and binding free energies to enhance precision and incorporate conformational changes in both protein and ligands, which are limited in rigid docking.

A typical IFD workflow began by defining the grid box around the centroid of the native ligand at the binding pocket of the 0X1 co-crystallized ligand and the 4GDY structure. Up to 20 poses per ligand were produced for Prime refinement, scaling van der Waals radii to 0.7 for the receptor and 0.5 for the ligand. Following Prime-based side-chain optimization and minimization, the refined poses were re-docked using Glide SP.

Molecular dynamics (MD) simulation

A 100 ns molecular dynamics simulation was run to examine the stability of the two best complexes, involving herbacetin and (-)-Epicatechin, within the KAT-II active site. Initial binding orientations and interaction types were explored via Glide XP docking. Simulation outcomes were analyzed through root mean square deviation (RMSD), root mean square fluctuation (RMSF), and protein-ligand interaction histograms. RMSD quantifies structural conformational stability by tracking average atomic displacements relative to a reference frame.

The Protein Preparation Wizard was applied to set up the KAT-II complexes with the two top candidates for MD. Simulations were executed using Desmond-2018, producing 1000 frames over 100 ns. The systems were solvated in a 10 Å × 10 Å × 10 Å SPC water box under orthorhombic boundary conditions. The System Builder added 0.15 M NaCl for neutralization. Energy minimization involved 2000 steepest descent steps with a 9 Å van der Waals cutoff. The NPT ensemble maintained 300 K temperature and 1.01325 bar pressure. All simulations used the OPLS3e force field [18].

In vitro enzyme inhibition and kinetic analysis

The assay for KAT-II inhibition followed the protocol described by Lu *et al*. [19], with minor adjustments. The two leading candidates were tested in a fluorescence-based microplate assay for kynurenine aminotransferase activity. The 20 µL reaction volume included 20 nM recombinant human KAT-II, 1 mM L-KYN, 0.3 mM L-α-aminoadipic acid (AAD), 50 µM α-ketoglutaric acid, 3 mM NAD+, and 88 µg/mL glutamic dehydrogenase.

Herbacetin and (-)-Epicatechin, dissolved in DMSO, were evaluated at various concentrations after 30 min pre-incubation with the enzyme in 0.1 M phosphate buffer (pH 7.5) supplemented with 5 µM PLP. Kinetic measurements were recorded over 30 min. Inhibition percentages were calculated for each dose, and IC50 values were derived via four-parameter non-linear regression. The assay was confirmed with the known inhibitor PF-04859989, yielding an IC50 of 27.91 ± 1.83 nM, aligning with reported data from Maryška *et al.* [10].
Kinetic behavior of herbacetin and (-)-Epicatechin was assessed using Lineweaver–Burk double-reciprocal plots to determine inhibition mode. The protocol mirrored the inhibition assay, with L-Kyn substrate concentrations of 1.00, 0.80, 0.60, 0.40, and 0.20 mM, and inhibitor levels of 1.00, 10.00, and 20.00 µM for each compound. Competitive inhibition constants (Ki) were computed using GraphPad Prism (v8.4.0).

Cytotoxicity assay
Cell cytotoxicity was evaluated using the MTT assay, adapted from the protocol outlined by [20] with minor adjustments. The HepG2 cells were sourced from ECACC (European Collection of Authenticated Cell Cultures, Sigma-Aldrich, Germany). Cells were maintained in DMEM supplemented with 10% fetal bovine serum (FBS), 2 mM L-glutamine, 1 mM sodium pyruvate, 100 U/mL penicillin, 100 µg/mL streptomycin, and 250 µg/mL fungizone, under humidified conditions at 37 °C with 5% CO_2.
For subculturing, cells were washed with 2.5 mL PBS, detached using 1.5 mL of 0.25% trypsin-EDTA for 5 min at 37 °C, and pelleted by centrifugation at 1500 rpm for 6 min at 4 °C. The pellet was then resuspended in fresh medium after discarding the supernatant, with routine medium changes every two days. Experiments were conducted in 96-well plates using triplicate wells per compound, with the entire assay repeated three times.
Cell viability was measured via the MTT (3-(4,5-dimethylthiazol-2-yl)-2,5-diphenyltetrazolium bromide) reduction method. Cells were seeded at a density of 8000 cells per well in 0.1 mL medium. Herbacetin and (-)-Epicatechin (prepared in DMSO) were applied at concentrations ranging from 1 to 250 µM, followed by incubation at 37 °C for 72 h. Subsequently, 10 µL of 5 mg/mL MTT solution was added to each well, and plates were incubated for an additional 4 h at 37 °C. Absorbance of the formazan product was measured at 570 nm on a VERSAmax microplate reader.
Viability percentages for the tested compounds were plotted as a function of concentration, and IC_{50} values were derived graphically through curve-fitting analysis.

Statistical evaluation
Data analysis was conducted with GraphPad Prism version 8.4.0. All experiments were performed in triplicate (n = 3), and results are expressed as mean ± standard deviation (SD).

Results and Discussion

Advances in computational chemistry and drug discovery have increasingly relied on in silico methods to streamline the identification of bioactive molecules with targeted activity against specific proteins [21]. Such approaches offer efficiency and reduced costs in early-stage screening.
In this study, computational techniques were employed to pinpoint two flavonoid compounds as novel, non-toxic KAT-II inhibitors derived from natural sources. Subsequent laboratory experiments confirmed their potency and lack of cytotoxicity.

Molecular docking, MMGBSA, and ADMET analysis
Techniques such as molecular docking, binding free energy estimation, and absorption-distribution-metabolism-excretion-toxicity (ADMET) profiling are essential for high-throughput evaluation of compound libraries to select viable drug leads.
The docking protocol was first verified by redocking the co-crystallized ligand using the Glide XP module. This assessment compared the predicted lowest-energy pose against the experimental structure. The calculated root mean square deviation (RMSD) was 1.473 Å, well below the 2.0 Å threshold that signifies a dependable docking methodology [18].
Following application of Lipinski's and Veber's filters to refine the compound set [14, 15], 231 candidates advanced to extra-precision (XP) docking. Results were then narrowed using a docking score threshold of −7.00 kcal/mol to prioritize superior binders [22, 23].

Docking scores for the initial XP screen spanned −1.81 to −8.66 kcal/mol. Only five compounds exceeded −7 kcal/mol, whereas the majority fell between −1.81 and −6.82 kcal/mol and were excluded from deeper evaluation. The leading candidates—herbacetin, (-)-Epicatechin, melilotoside, sakakin, and eriodictyol—exhibited strong binding interactions and high affinity scores **(Table 1).**

Table 1. Energy-based interactions detail of the top five hits.

Compound	Glide Emodel (kcal/mol)	Docking Score (kcal/mol)	MMGBSA ΔG Bind (kcal/mol)	Number of Hydrogen Bonds	Hydrogen Bond Interactions and Distances (Å)
Herbacetin	−44.95	−8.66	−50.30	5	Asn202 (3.00 Å), Ser117 (2.01 Å), Ser260 (1.98 Å), Ser262 (2.01 Å), Lys263 (2.54 Å)
(−)-Epicatechin	−39.32	−8.16	−51.35	4	Tyr233 (1.82 Å), Tyr142 (2.00 Å), Asp230 (1.93 Å), Ser117 (2.02 Å)
Melilotoside	−51.41	−7.91	−34.34	6	Tyr233 (1.89 Å), Lys263 (2.74 Å), Asp230 (1.77 Å), Ser117 (2.21 Å), Ser260 (1.99 Å), Arg270 (1.73 Å)
Sakakin	−44.76	−7.84	−49.51	4	Tyr142 (2.12 Å), Ser117 (1.96 Å), Ser260 (2.07 Å), Ser262 (1.79 Å)
Eriodictyol	−42.53	−7.63	−51.33	4	Tyr233 (2.02 Å), Asn202 (2.09 Å), Ser260 (2.33 Å), Ser117 (2.02 Å)
PF-04859989 (reference inhibitor)	−28.88	−7.12	−38.41	3	Tyr233 (2.04 Å), Asn202 (2.73 Å), Asp230 (1.81 Å)

Figure 1 and **Table 1** depict the ligand-binding sites, highlighting the key amino acid residues participating in hydrogen bonding and hydrophobic contacts, thereby offering deeper understanding of the molecular interactions between KAT-II and the chosen compounds.

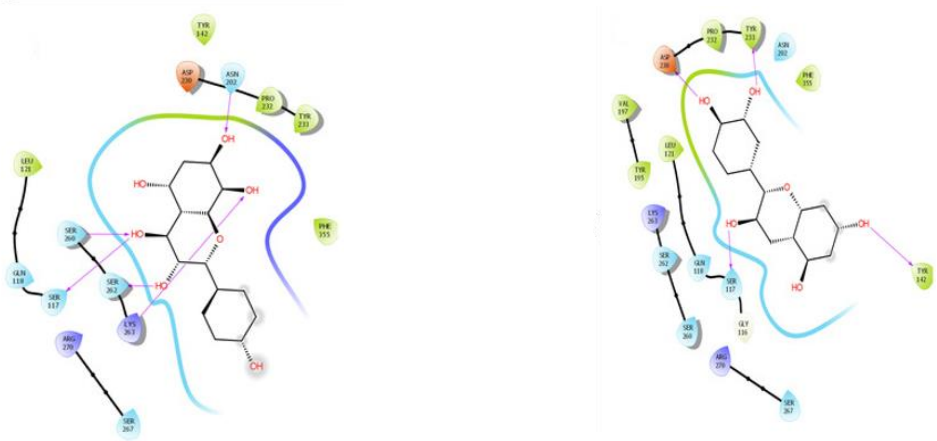

a) b)

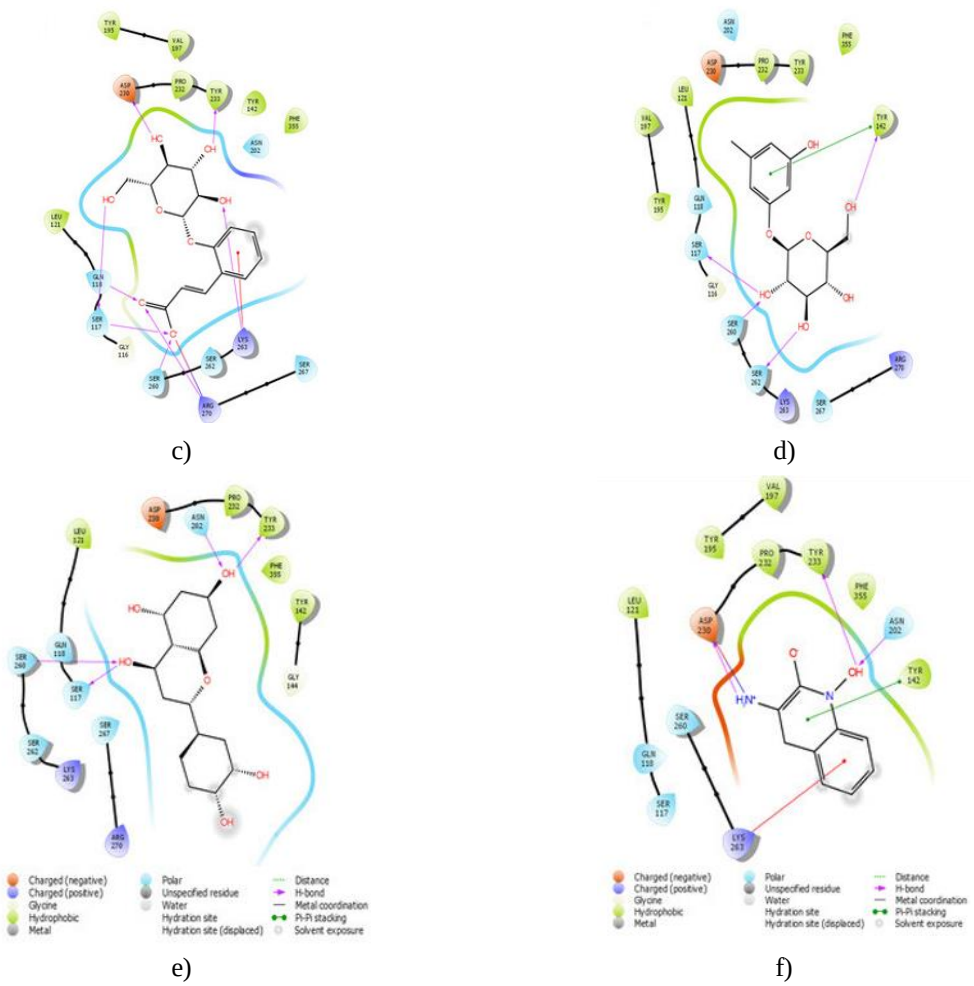

Figure 1. Two-dimensional representations of interactions between the top candidate molecules and the reference inhibitor within the KAT-II binding pocket: (a) herbacetin, (b) (−)-epicatechin, (c) melilotoside, (d) sakakin, (e) eriodictyol, (f) PF-04859989.

Herbacetin established hydrogen bonds with key binding site residues including Asn202, Ser117, Ser260, Ser262, and Lys263 **(Figure 1a).** The other natural compounds—(−)-epicatechin, melilotoside, sakakin, and eriodictyol—demonstrated strong binding to KAT-II, achieving docking scores of −8.16, −7.91, −7.84, and −7.63 kcal/mol, respectively **(Table 1).** (−)-Epicatechin engaged in hydrogen bonding with Tyr233, Tyr142, Asp230, and Ser117 **(Figure 1b).** Melilotoside formed hydrogen bonds with Tyr233, Lys263, Asp230, Ser117, Ser260, and Arg270 **(Figure 1c),** whereas sakakin bonded with Tyr142, Ser117, Ser260, and Ser262 **(Figure 1d).** Eriodictyol, ranked fifth, displayed hydrogen bonds with Tyr233, Asn202, Ser260, and Ser117 **(Figure 1e)**. Beyond hydrogen bonding, various hydrophobic contacts were also evident with the protein target **(Figure 1).**

The docking data indicate that the superior inhibitory potential of herbacetin and (−)-epicatechin arises from their extensive hydrogen bonding with active site residues of KAT-II. These leading compounds exhibited hydrogen bonding patterns comparable to those of the known inhibitor 17-sulfate of estradiol disulfate, effectively targeting conserved residues such as Asn202 and Lys263 [6, 7]. Prior research has shown that interactions with essential binding site residues like Asn202 and Tyr233 are vital for engagement with both the substrate and the cofactor PLP [7, 24, 25]. Furthermore, Lys263 is catalytically critical because of its direct interaction with PLP, contributing significantly to the efficacy of KAT-II inhibitors [5, 6].

Hydrophobic interactions contributing to ligand stabilization involved conserved residues across herbacetin and the other compounds **(Table 1).** Notably, Tyr142 stands out as a particularly important residue for effective ligand binding.

Compounds exhibiting the highest Glide scores were subjected to MM-GBSA calculations to determine binding free energies and pinpoint the most potent candidates. The top five docking hits yielded binding free energies of

−50.30, −51.35, −34.34, −49.51, and −51.33 kcal/mol, respectively. In comparison, the MMGBSA binding free energy for the reference inhibitor PF-04859989 was −38.41 kcal/mol.

Evaluation of drug-likeness and ADMET properties

Selection of the top five compounds was based on their docking scores, specific ligand–protein contacts, and MMGBSA binding affinities relative to the reference compound PF-04859989.

Predicted human oral bioavailability for these molecules and the reference inhibitor varied between 36.716% and 61.197%. The compounds also showed favorable octanol–water partition coefficients (QP log Po/w), with values falling in the range of −0.814 to 0.416 **(Table 2).**

Table 2. ADME properties of the top five molecules.

Parameter	Herbacetin	(−)-Epicatechin	Melilotoside	Sakakin	Eriodictyol	PF-04859989
Hydrogen bond donors	4.000	5.000	5.000	5.000	3.000	3.000
Hydrogen bond acceptors	5.250	5.450	11.250	10.000	4.750	5.200
Human oral absorption (%)	53.100	61.197	36.716	56.651	62.522	59.55
QP log Po/w	0.416	0.454	−0.520	−0.814	0.875	−0.525
QP log S	−2.846	−2.518	−1.886	−1.751	−3.930	−0.233
QPPCaco (nm/s)	27.141	58.241	5.200	84.334	50.276	98.591
QP log BB	−2.318	−1.815	−2.682	−1.866	−1.797	−0.325
Lipinski's Rule of Five violations	0	0	0	0	0	0

Hydrogen bond donors (HB donor) and acceptors (HB acceptor); human oral absorption percentage (>80% considered high, <25% considered poor); QP log Po/w (recommended range: −2.0 to 6.5); QP log S (predicted aqueous solubility, recommended: −6.5 to 0.5); QPPCaco (predicted apparent Caco-2 cell permeability in nm/s; <25 poor, >500 excellent); QP log BB (predicted brain/blood partition coefficient; recommended: −3.0 to 1.2); Lipinski's Rule of Five violations (maximum of 4 allowed; 0 indicates full compliance).

The predicted brain/blood partition coefficients (QP log BB) for the compounds ranged from −2.318 to −0.325, which lies within the recommended limits. Caco-2 cell permeability values (in nm/s) varied between 5.200 and 98.591, suggesting favorable membrane penetration capabilities for these molecules **(Table 2).**

With the exception of melilotoside, the pharmacokinetic properties of all evaluated compounds remained within the recommended ranges for potential human application, as detailed in **Table 2**. Although melilotoside exhibited low Caco-2 permeability, all compounds complied with Lipinski's Rule of Five (zero violations), indicating strong drug-like characteristics and considerable promise as therapeutic candidates.

Acute toxicity profiles of the leading compounds were assessed using the ProTox-II web server. Key toxicity endpoints, such as oral LD50 values, toxicity class, hepatotoxicity, neurotoxicity, immunotoxicity, and mutagenicity, were examined **(Table 3).**

Table 3. Toxicity assessment of the candidate compounds.

Parameters		Herbacetin	(-)-Epicatechin	Melilotoside	Sakakin	Eriodictyol	PF-04859989
LD_{50} (mg/kg)		3919	10,000	1500	1380	2000	500
Prediction class		Class 5	Class 6	Class 4	Class 4	Class 4	Class 4
Hepatotoxicity	Prediction	Inactive	Inactive	Inactive	Inactive	Inactive	Inactive
	Probability	0.69	0.72	0.82	0.92	0.67	0.53
Neurotoxicity	Prediction	Inactive	Inactive	Inactive	Inactive	Inactive	Active
	Probability	0.89	0.90	0.88	0.92	0.88	0.57
Immunotoxicity	Prediction	Inactive	Inactive	Active	Inactive	Inactive	Inactive
	Probability	0.92	0.96	0.56	0.96	0.71	0.99
Mutagenicity	Prediction	Active	Inactive	Inactive	Inactive	Inactive	Active

	Probability	0.51	0.55	0.78	0.76	0.59	0.62
Prediction accuracy		70.97%	100%	69.26%	69.26%	69.26%	68.07%

Prediction class: class 4 (harmful if swallowed (300 < LD50 ≤ 2000); class 5: may be harmful (slightly toxic) if swallowed (2000 < LD50 ≤ 5000); class 6: non-toxic (LD50 > 5000) [17].

Toxicity classification (ranging from class 1 (highly toxic) to class 6 (non-toxic)) indicated that herbacetin and (−)-epicatechin possessed favorable safety profiles, falling into classes 5 and 6, respectively. In contrast, the remaining compounds, along with the reference inhibitor PF-04859989, were categorized under class 4, suggesting a higher degree of toxicity [17].

With the exception of herbacetin, which displayed mild (potentially negligible) mutagenicity relative to the reference inhibitor, none of the evaluated compounds exhibited hepatotoxicity, carcinogenicity, cytotoxicity, immunotoxicity, or mutagenicity. These results further support their overall safety for prospective applications.

Induced fit docking studies

Induced fit docking (IFD) was performed on the two leading candidates, with PF-04859989 serving as the reference inhibitor. The analysis showed that herbacetin achieved the highest IFD score of −849.344 kcal/mol, closely followed by (−)-epicatechin at −844.853 kcal/mol. Both values surpassed the IFD score of −843.776 kcal/mol obtained for PF-04859989.

The ligand conformations produced by IFD exhibited only slight deviations from those derived from rigid receptor docking. Nevertheless, certain interactions were newly formed or removed compared to the extra precision (XP) docking results, while others persisted unchanged. For herbacetin, additional hydrogen bonds emerged with Ser267 and Asp230, whereas the original hydrogen bonds with Ser260 and Lys263 were no longer present following IFD. Hydrophobic contacts and the remaining hydrogen bonds were preserved as in XP docking **(Figure 2a)**. In the case of (−)-epicatechin, novel hydrogen bonds developed with Asn202, Ser267, and Arg270, but interactions with Tyr142 and Tyr233 were lost **(Figure 2b).** The reference inhibitor PF-04859989 retained nearly identical interaction patterns to those from XP docking, gaining a new hydrogen bond with Gln118 and a positive charge interaction with Arg399 **(Figure 2c)**. Overall, these observations suggest that the two top compounds exert stronger inhibitory activity than PF-04859989 due to superior engagement with the KAT-II binding pocket.

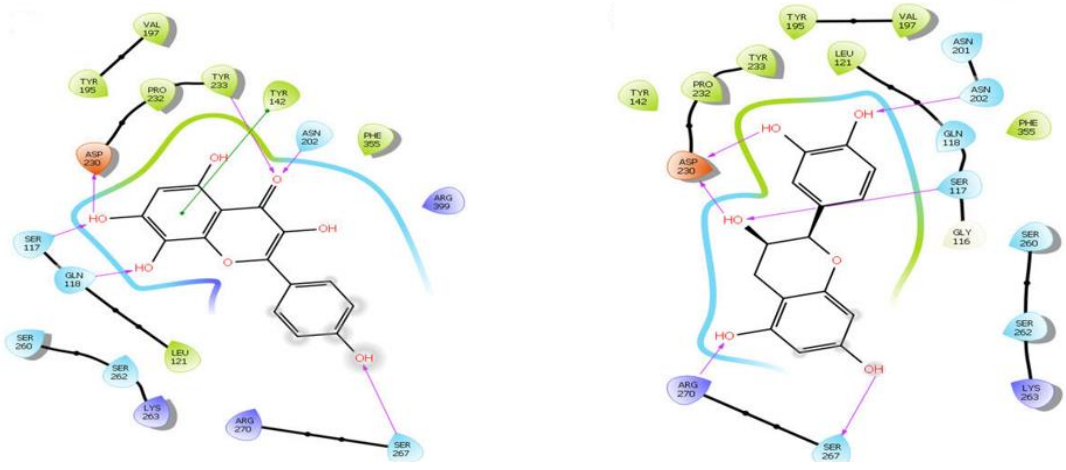

a) b)

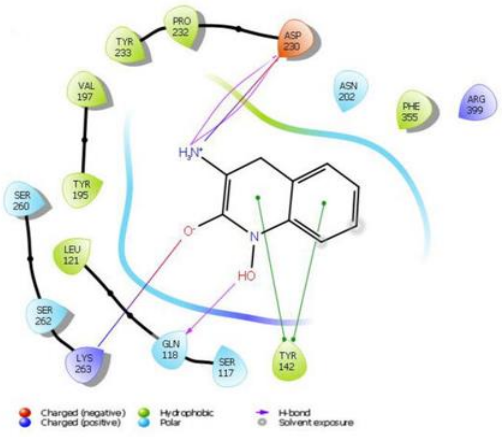

c)

Figure 2. Two-dimensional interaction diagrams from induced fit docking for: (a) herbacetin; (b) (−)-epicatechin; (c) PF-04859989.

Molecular dynamics simulation

Examination of the RMSD plot indicates that the herbacetin–KAT-II complex exhibits limited fluctuations in RMSD values over the course of the simulation. The system achieved stability after approximately 20 ns and maintained this equilibrium until completion, with the highest RMSD reaching only 2 Å **(Figure 3a).** This value lies well within the generally accepted range for stable protein–ligand complexes (1–3 Å), underscoring the robust and consistent binding behavior of herbacetin with KAT-II and providing valuable insights into the dynamics of their interaction.

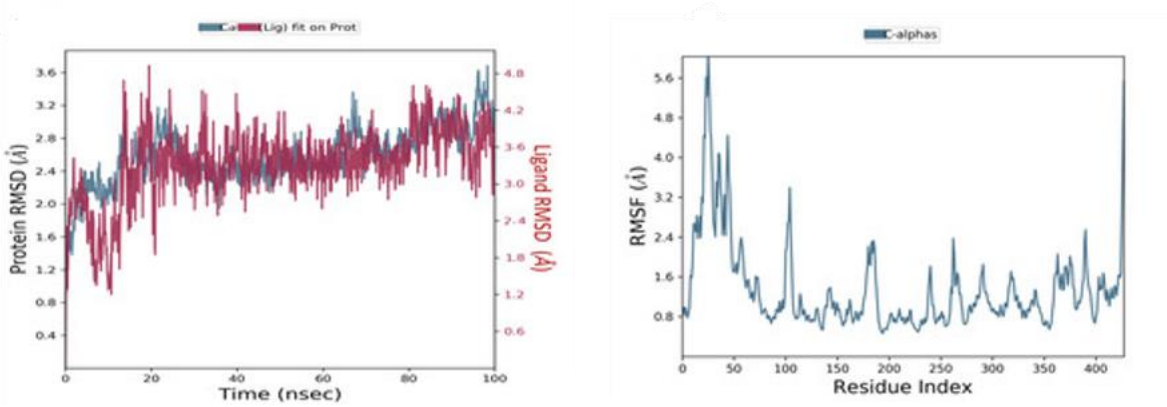

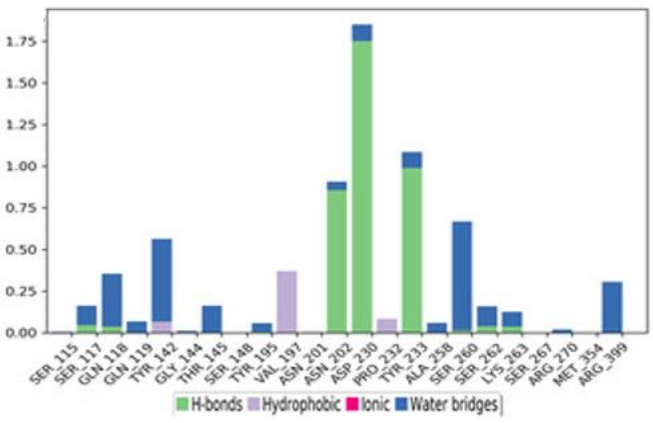

c)

Figure 3. Molecular dynamics simulation results for the herbacetin–KAT-II complex: (a) RMSD trajectory of the complex, (b) RMSF profile of the complex, (c) interaction histogram for the herbacetin–KAT-II complex.

The (−)-epicatechin–KAT-II complex displayed relatively low RMSD fluctuations overall, reflecting consistent conformational stability throughout the simulation period. Despite an initial RMSD peak around 4 Å and some variability observed between 0 and 60 ns, the system reached equilibrium after 85 ns **(Figure 4a),** at which point both protein backbone and ligand RMSD values remained steady.

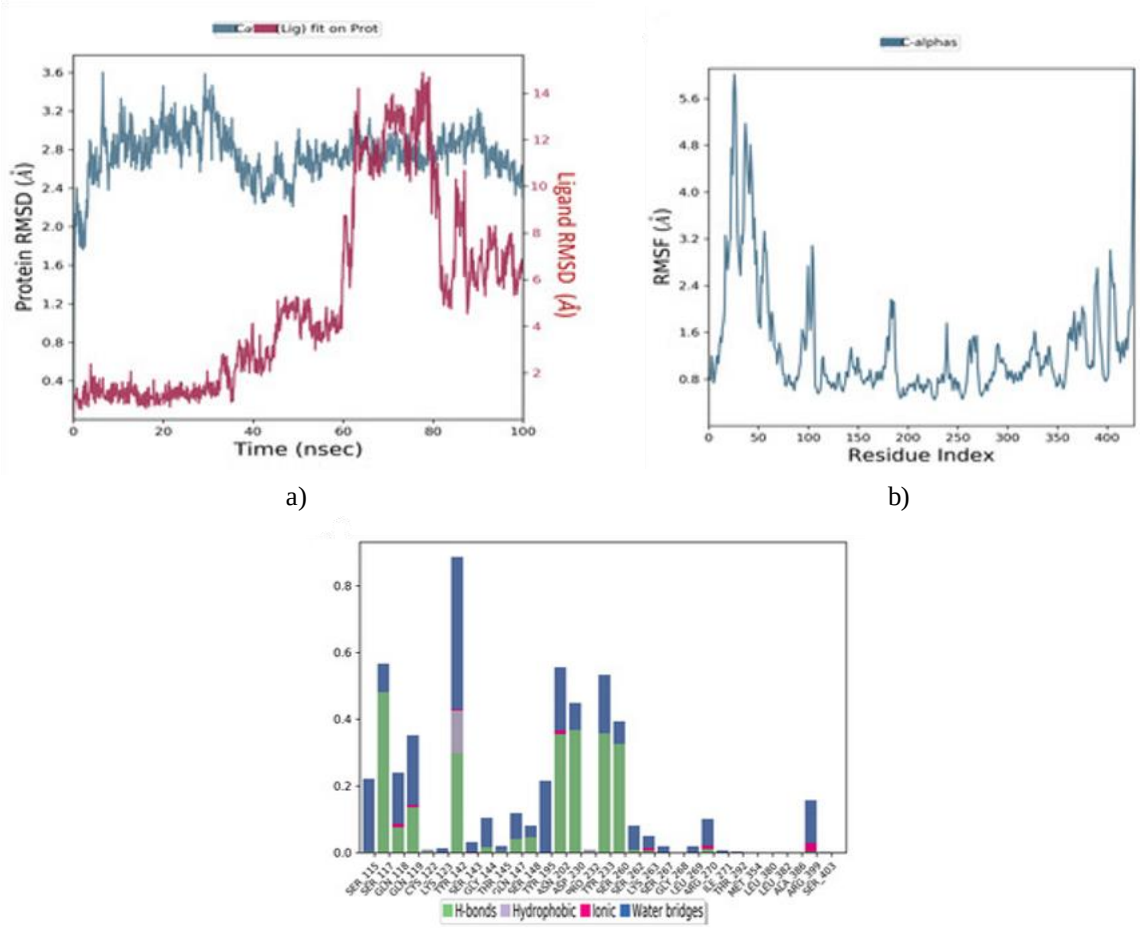

a) b)

c)

Figure 4. Molecular dynamics simulation results for the (−)-epicatechin–KAT-II complex: (a) RMSD trajectory of the complex, (b) RMSF profile of the complex, (c) interaction histogram for the (−)-epicatechin–KAT-II complex.

Root mean square fluctuation (RMSF) analyses were performed to evaluate the flexibility of individual residues in the docked complexes. As shown in **Figures 3b and 4b**, the N- and C-terminal regions displayed greater fluctuations compared to the rest of the protein structure. Elevated peaks correspond to regions of higher flexibility, whereas lower values reflect enhanced stability of the complexes over the course of the simulation. Reduced fluctuations are indicative of the system reaching equilibrium [18, 26].

RMSF values were determined for KAT-II in complex with the two leading drug candidates. Throughout the 100 ns simulation, RMSF profiles showed no substantial variations, and average RMSF values remained steady across all systems **(Figures 3b and 4b).**

Molecular dynamics simulations highlighted that the top candidate herbacetin maintained hydrogen bonds with residues Tyr233, Asn202, and Asp230 **(Figure 3c).** Additionally, hydrophobic interactions were observed with Tyr142, Ser260, and Arg399. For (−)-epicatechin, persistent contacts with key active site residues of KAT-II included hydrogen bonding to Ser117, Tyr142, Tyr233, Asn202, and Asp230, along with hydrophobic interactions involving Ser115 and Tyr195 **(Figure 4c).**

In vitro enzyme inhibition and kinetic studies

Herbacetin and (−)-epicatechin demonstrated notable inhibitory activity against KAT-II at the tested concentrations, yielding IC_{50} values of 5.98 ± 0.18 µM and 8.76 ± 0.76 µM, respectively **(Figures 5a and 5b).** In comparison, the reference compound PF-04859989 exhibited superior potency with an IC_{50} of 27.91 ± 1.81 nM ($p < 0.05$). Kinetic characterization revealed that, unlike PF-04859989 which forms an irreversible adduct with PLP, both herbacetin and (−)-epicatechin act as reversible inhibitors. This was substantiated by experiments in which increasing PLP concentrations in the assay reduced the inhibitory effects of these compounds, consistent with a competitive mechanism [6, 18].

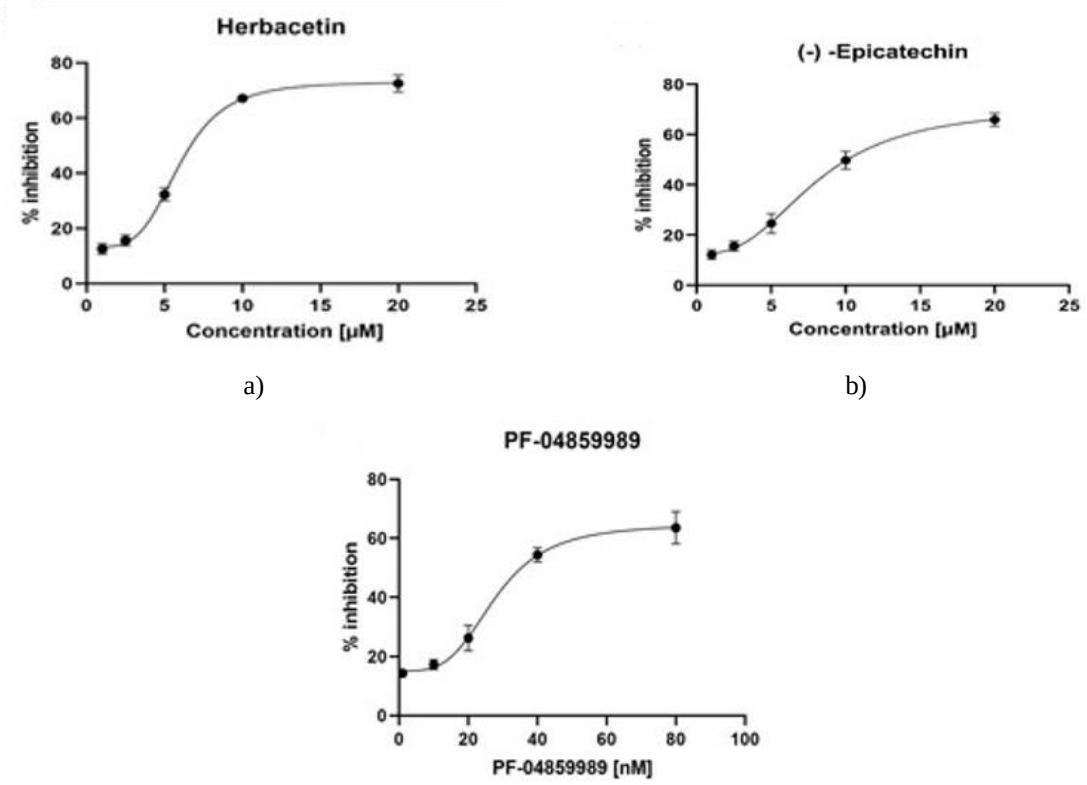

a) b)

c)

Figure 5. Dose-dependent inhibitory effects of (a) herbacetin, (b) (−)-epicatechin, and (c) PF-04859989 on KAT-II activity. All assays were conducted in triplicate, and data were analyzed and graphed using GraphPad Prism version 8.4.0.

Kinetic analyses revealed that both herbacetin and (−)-epicatechin function as competitive inhibitors, as evidenced by an increase in the apparent Michaelis constant (Km) with rising inhibitor concentrations while the maximum velocity (Vmax) remained constant **(Figures 6a and 6b)**. In contrast, the reference compound PF-04859989 exhibited non-competitive inhibition, characterized by a reduction in Vmax without alteration of Km **(Figure 7c).**

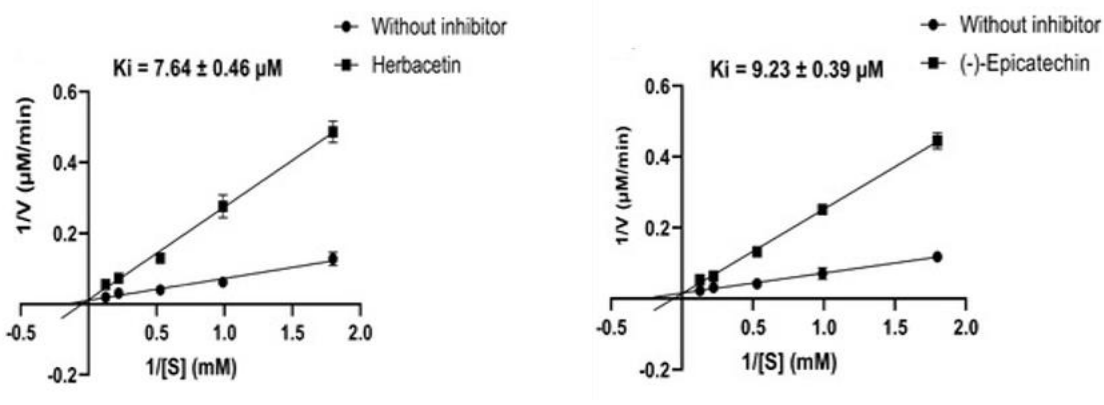

a) b)

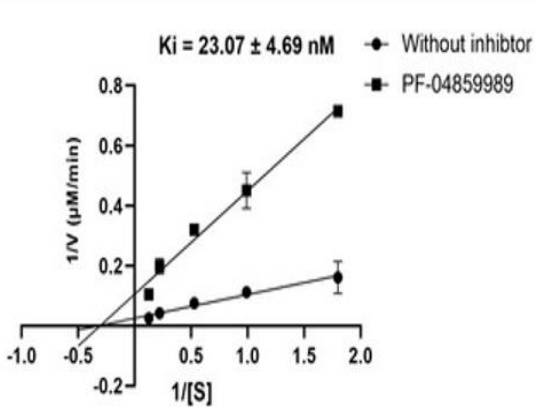

c)

Figure 6. Lineweaver–Burk plots illustrating the inhibition kinetics of herbacetin and (−)-epicatechin against KAT-II. Kinetic parameters for (a) herbacetin, (b) (−)-epicatechin, and (c) PF-04859989 were determined through Lineweaver–Burk double-reciprocal analysis. All assays were conducted in triplicate, with results expressed as mean ± standard deviation.

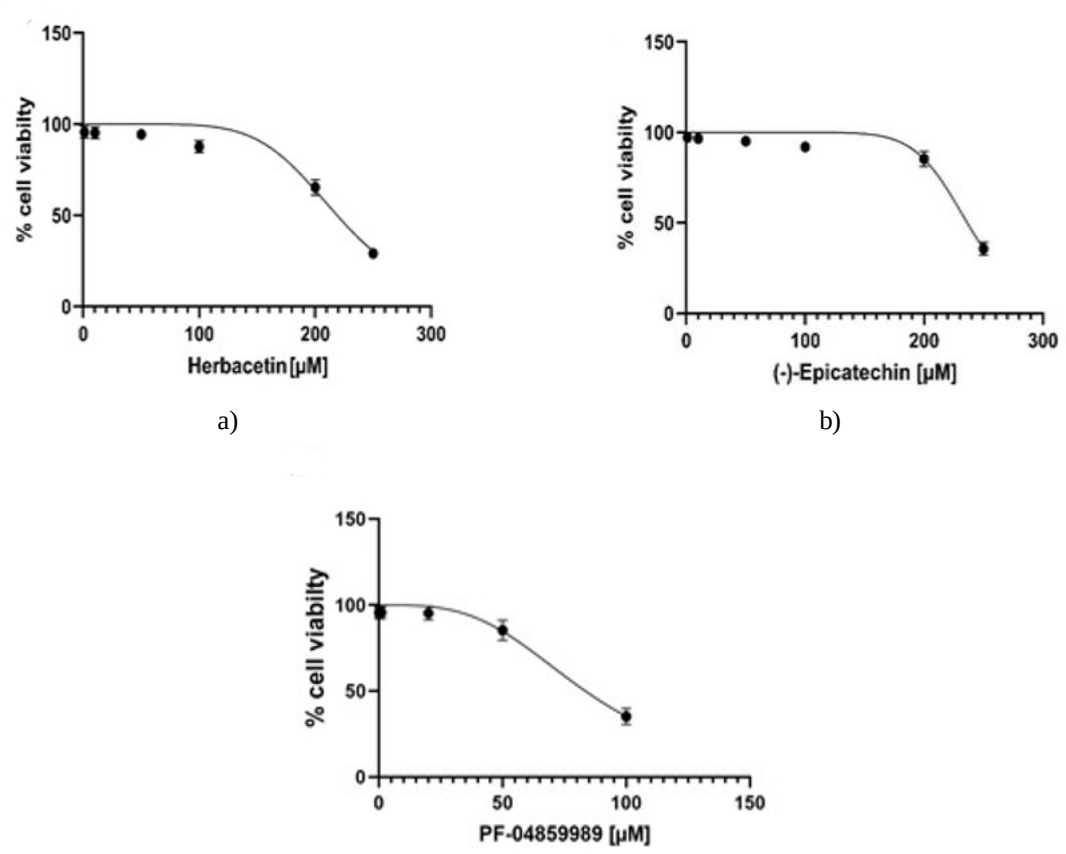

a) b)

c)

Figure 7. Cell viability (%) in HepG2 cells determined by MTT assay following 72 h treatment with (a) herbacetin, (b) (−)-epicatechin, and (c) PF-04859989.

The determined IC_{50} values clearly indicate that herbacetin and (−)-epicatechin are potent inhibitors of KAT-II, outperforming the synthetic reversible inhibitor NS-1502 (IC_{50}: 315 µM) and the irreversible inhibitor BFF-122 (IC_{50}: 15–20 µM), both of which were developed based on a kynurenine scaffold [6, 27, 28]. Both selected natural compounds displayed reversible inhibition characteristics: increasing PLP concentrations reduced their inhibitory potency, confirming competition with the cofactor. This differs from the irreversible mechanism of the positive control PF-04859989, whose activity remained unaffected by varying PLP levels. Similarly, the inhibition pattern

observed for these reversible inhibitors aligns with that of several recently reported natural KAT-II inhibitors, such as glycyrrhizic acid (IC_{50}: 4.51 ± 0.20 μM), glycyrrhetinic acid (IC_{50}: 6.96 ± 0.37 μM), and carbenoxolone (IC_{50}: 3.90 ± 0.37 μM), all of which target PLP reversibly [29].
Thus, we have discovered two novel natural KAT-II inhibitors that demonstrate superior performance over previously known inhibitors, especially in terms of their advantageous pharmacokinetic properties—a factor not adequately addressed in earlier investigations.

Cytotoxicity assessment
The effects of varying concentrations (1–250 μM) of the two leading compounds on cell viability were evaluated in human hepatocellular carcinoma (HepG2) cells using the MTT assay. Herbacetin and (−)-epicatechin exerted only minor effects on cell proliferation, with IC_{50} values of 218.90 ± 4.53 μM and 236.40 ± 2.53 μM, respectively **(Figures 7a and 7b).** In comparison, the reference inhibitor PF-04859989 displayed greater cytotoxicity, with an IC_{50} of 83.49 ± 2.86 μM ($p < 0.05$) **(Figure 7c).** These findings suggest that the natural compounds exhibit negligible cytotoxicity toward HepG2 cells, even at concentrations exceeding 200 μM.
Results from both computational modeling and in vitro assays support the existence of interactions between the investigated compounds and the target protein. Nevertheless, comprehensive additional experimental studies are required to establish their true pharmacological potential. The computational predictions presented here should be regarded as hypotheses rather than conclusive proof of clinical efficacy. Advancing these candidates toward viable KAT-II inhibitors for clinical use will necessitate in vivo evaluations of safety, pharmacokinetics, and pharmacodynamics.

Conclusion

This investigation combined computational approaches with in vitro kinetic experiments to discover novel, safe inhibitors of KAT-II. Molecular docking highlighted herbacetin and (-)-Epicatechin as promising candidates, both demonstrating strong binding affinities toward KAT-II. Molecular dynamics simulations corroborated the docking outcomes, confirming stable complexes and sustained favorable interactions over the simulation period for both compounds. The results further indicated favorable ADME profiles and low predicted toxicity.
In addition, in vitro studies confirmed that these molecules function as competitive, reversible inhibitors with significant potency against KAT-II, while exhibiting no adverse effects on cell viability. These findings position herbacetin and (-)-Epicatechin as strong candidates for schizophrenia therapy; however, additional preclinical investigations are required to advance their development.

Acknowledgments: None

Conflict of Interest: None

Financial Support: None

Ethics Statement: None

References

1. Barazorda-Ccahuana HL, Zevallos-Delgado C, Valencia DE, Gómez B. Molecular dynamics simulation of kynurenine aminotransferase type II with nicotine as a ligand: A possible biochemical role of nicotine in schizophrenia. ACS Omega. 2019;4:710–7.
2. Almulla AF, Vasupanrajit A, Tunvirachaisakul C, Al-Hakeim HK, Solmi M, Verkerk R, et al. The tryptophan catabolite or kynurenine pathway in schizophrenia: Meta-analysis reveals dissociations between central, serum, and plasma compartments. Mol Psychiatry. 2022;27:3679–91.
3. Gotina L, Seo SH, Kim CW, Lim SM, Pae AN. Pharmacophore-based virtual screening of novel competitive inhibitors of the neurodegenerative disease target kynurenine-3-monooxygenase. Molecules. 2021;26:3314.

4. Linderholm KR, Alm MT, Larsson MK, Olsson SK, Goiny M, Hajos M, et al. Inhibition of kynurenine aminotransferase II reduces activity of midbrain dopamine neurons. Neuropharmacology. 2016;102:42–7.
5. Dounay AB, Anderson M, Bechle BM, Campbell BM, Claffey MM, Evdokimov A, et al. Discovery of brain-penetrant, irreversible kynurenine aminotransferase II inhibitors for schizophrenia. ACS Med Chem Lett. 2012;3:187–92.
6. Jayawickrama GS, Nematollahi A, Sun G, Gorrell MD, Church WB. Inhibition of human kynurenine aminotransferase isozymes by estrogen and its derivatives. Sci Rep. 2017;7:17559.
7. Jayawickrama GS, Nematollahi A, Sun G, Church WB. Improvement of kynurenine aminotransferase-II inhibitors guided by mimicking sulfate esters. PLoS ONE. 2018;13:e0196404.
8. Cherrak SA, Merzouk H, Mokhtari-Soulimane N. Potential bioactive glycosylated flavonoids as SARS-CoV-2 main protease inhibitors: A molecular docking and simulation studies. PLoS ONE. 2020;15:e0240653.
9. Dias MC, Pinto DC, Silva AM. Plant flavonoids: Chemical characteristics and biological activity. Molecules. 2021;26:5377.
10. Maryška M, Svobodová L, Dehaen W, Hrabinová M, Rumlová M, Soukup O, et al. Heterocyclic cathinones as inhibitors of kynurenine aminotransferase II—Design, synthesis, and evaluation. Pharmaceuticals. 2021;14:1291.
11. Henderson JL, Sawant-Basak A, Tuttle JB, Dounay AB, McAllister LA, Pandit J, et al. Discovery of hydroxamate bioisosteres as KAT II inhibitors with improved oral bioavailability and pharmacokinetics. MedChemComm. 2013;4:125–9.
12. Berman HM, Westbrook J, Feng Z, Gilliland G, Bhat TN, Weissig H, et al. The protein data bank. Nucleic Acids Res. 2000;28:235–42.
13. Kim S, Chen J, Cheng T, Gindulyte A, He J, He S, et al. PubChem 2023 update. Nucleic Acids Res. 2023;51:D1373–D1380.
14. Lipinski CA. Drug-like properties and the causes of poor solubility and poor permeability. J Pharmacol Toxicol Methods. 2000;44:235–49.
15. Veber DF, Johnson SR, Cheng HY, Smith BR, Ward KW, Kopple KD. Molecular properties that influence the oral bioavailability of drug candidates. J Med Chem. 2002;45:2615–23.
16. Derardja I, Rebai R, Toumi ME, Kebaili FF, Boudah A. Identification of New Potential Cyclooxygenase-2 Inhibitors Using Structure-Based Virtual Screening, Molecular Dynamics and Pharmacokinetic Modelling. In: Proceedings of the Biology and Life Sciences Forum, The 3rd International Electronic Conference on Biomolecules; 2024 Apr 23–25; Online. p. 6.
17. Banerjee P, Eckert AO, Schrey AK, Preissner R. ProTox-II: A webserver for the prediction of toxicity of chemicals. Nucleic Acids Res. 2018;46:W257–W263.
18. Rebai R, Carmena-Bargueño M, Toumi ME, Derardja I, Jasmin L, Pérez-Sánchez H, et al. Identification of potent inhibitors of kynurenine-3-monooxygenase from natural products: In silico and in vitro approaches. Heliyon. 2024;10:e30287.
19. Lu H, Kopcho L, Ghosh K, Witmer M, Parker M, Gupta S, et al. Development of a RapidFire mass spectrometry assay and a fluorescence assay for the discovery of kynurenine aminotransferase II inhibitors to treat central nervous system disorders. Anal Biochem. 2016;501:56–65.
20. Fettach S, Thari FZ, Hafidi Z, Karrouchi K, Bouathmany K, Cherrah Y, et al. Biological, toxicological and molecular docking evaluations of isoxazoline-thiazolidine-2,4-dione analogues as new class of anti-hyperglycemic agents. J Biomol Struct Dyn. 2023;41:1072–84.
21. Das AP, Agarwal SM. Recent advances in the area of plant-based anti-cancer drug discovery using computational approaches. Mol Divers. 2024;28:901–25.
22. Moitra P. A combinatorial approach of structure-based virtual screening and molecular dynamics simulation towards the discovery of a highly selective inhibitor for VP9 coat protein of Banna virus. Bioorganic Chem. 2019;86:15–27.
23. Madhavaram M, Nampally V, Gangadhari S, Palnati MK, Tigulla P. High-throughput virtual screening, ADME analysis, and estimation of MM/GBSA binding-free energies of azoles as potential inhibitors of Mycobacterium tuberculosis H37Rv. J Recept Signal Transduct. 2019;39:312–20.

24. Noorbakhsh A, Hosseininezhadian Koushki E, Farshadfar C, Ardalan N. Designing a natural inhibitor against human kynurenine aminotransferase type II and a comparison with PF-04859989: A computational effort against schizophrenia. J Biomol Struct Dyn. 2022;40:7038–51.
25. Dounay AB, Anderson M, Bechle BM, Evrard E, Gan X, Kim JY, et al. PF-04859989 as a template for structure-based drug design: Identification of new pyrazole series of irreversible KAT II inhibitors with improved lipophilic efficiency. Bioorg Med Chem Lett. 2013;23:1961–6.
26. Akbar S, Das S, Iqubal A, Ahmed B. Synthesis, biological evaluation and molecular dynamics studies of oxadiazine derivatives as potential anti-hepatotoxic agents. J Biomol Struct Dyn. 2022;40:9974–91.
27. Nematollahi A, Sun G, Jayawickrama GS, Hanrahan JR, Church WB. Study of the activity and possible mechanism of action of a reversible inhibitor of recombinant human KAT-2: A promising lead in neurodegenerative and cognitive disorders. Molecules. 2016;21:856.
28. Rossi F, Schwarcz R, Rizzi M. Curiosity to kill the KAT (kynurenine aminotransferase): Structural insights into brain kynurenic acid synthesis. Curr Opin Struct Biol. 2008;18:748–55.
29. Yoshida Y, Fujigaki H, Kato K, Yamazaki K, Fujigaki S, Kunisawa K, et al. Selective and competitive inhibition of kynurenine aminotransferase 2 by glycyrrhizic acid and its analogues. Sci Rep. 2019;9:10243.